High pressure dissociation of CaTiO3 perovskite into CaO and CaTi2O5

B Truffet, G Fiquet, G Morard, M A Baron, F Miozzi, M Harmand, A Ravasio, M Mezouar, F Guyot

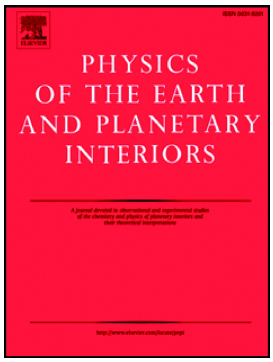

High pressure dissociation of CaTiO3 perovskite into CaO and CaTi2O5

B. Truffet, G. Fiquet, G. Morard, M.A. Baron, F. Miozzi, M. Harmand, A. Ravasio, M. Mezouar, F. Guyot

PII: S0031-9201(22)00129-7

DOI: https://doi.org/10.1016/j.pepi.2022.106968

Reference: PEPI 106968

To appear in: *Physics of the Earth and Planetary Interiors*

Received date: 27 December 2021

Revised date: 11 October 2022

Accepted date: 1 November 2022

Please cite this article as: B. Truffet, G. Fiquet, G. Morard, et al., High pressure dissociation of CaTiO3 perovskite into CaO and CaTi2O5, *Physics of the Earth and Planetary Interiors* (2022), https://doi.org/10.1016/j.pepi.2022.106968

High pressure dissociation of $CaTiO_3$ perovskite into CaO and $CaTi_2O_5$

B. Truffet[1*], G. Fiquet[1], G. Morard[1,2], M.A. Baron[1], F. Miozzi[1,3], M. Harmand[1], A. Ravasio[4], M. Mezouar[5], F. Guyot[1,6]

[1.] Sorbonne Université, UMR CNRS 7590, Muséum National d'Histoire Naturelle, Institut de Minéralogie, Physique des Matériaux et Cosmochimie, IMPMC, 4 Place Jussieu, 75005 Paris

[2.] Now at Univ. Grenoble Alpes, Univ. Savoie Mont Blanc, CNRS, IRD, Univ. Gustave Eiffel, ISTerre, 38000 Grenoble, France

[3.] Now at Earth and Planets Laboratory, Carnegie Institution for Science, Washington, DC, USA

[4.] Laboratoire pour l'Utilisation des Lasers Intenses (LULI) Ecole Polytechnique, CNRS, Sorbonne Université, CEA, Palaiseau, France

[5] European Synchrotron Radiation Facility, ESRF, Grenoble

[6.] Institut Universitaire de France (IUF)

Highlights:

- Phase diagram of the calcium titanate perovskite $CaTiO_3$ up to 170 GPa and 4500 K.
- Thermal equation of state of the orthorhombic (*Pbnm*) perovskite $CaTiO_3$.
- Dissociation of the $CaTiO_3$ perovskite into CaO and $CaTi_2O_5$ without going through a post-perovskite phase

Key words:

Perovskite, $CaTiO_3$, Equation of State, Dissociation, High-pressure

Abstract

In this study, we investigated phase transformations of $CaTiO_3$ perovskite using x-ray diffraction at high pressure and high temperature up to 170 GPa and 4500 K in a laser-heated diamond-anvil cell. We report a high-pressure dissociation of $CaTiO_3$ into CaO-B2 and $CaTi_2O_5$ with a monoclinic *P2/m* structure, instead of the expected transformation of the orthorhombic distorted perovskite structure into a post-perovskite phase. We propose that this transition may be favored by the *B1* to *B2* phase change of CaO at around 60 GPa. In order to

provide additional information on the high pressure properties of $CaTiO_3$ perovskite, we measured its melting temperature using CO_2 laser heated diamond anvil cell up to 55 GPa yielding a fit of the melting curve to a Kraut-Kennedy empirical law according to : $Tm\ (K) = 2188 * [1 + 4.23 * (\Delta V/V_0)]$. To provide some further insight into the thermodynamic properties of $CaTiO_3$, we determined the P-V-T equation of state of the orthorhombic mineral perovskite, fitted by using a third order Birch-Murnaghan equation of state and a Berman thermal expansion model. The fit of the data yields to K_0 = 180.6(4) GPa, K'_0 = 4 (fixed), $\partial K/\partial T$ = -0.022(1) GPa K^{-1}, α_1 = 3.25(5) x 10^{-5} K^{-1}, α_2 = 1.3(1) x 10^{-8} K^{-2}

Plain language summary

Among 5000+ discovered exoplanets, some of them are classified as super-Earths. Based on their average densities derived from mass/radius observations, these planets are expected to be rocky but have a larger radius than that of the Earth and thus higher internal pressures. Bridgmanite, the orthorhombic perovskite structured compound with $(Mg,Fe)SiO_3$ composition, considered to be the most abundant mineral in the Earth's rocky mantle is likely abundant in super-Earths as well. Atomistic calculations have predicted that $MgSiO_3$ dissociates between 1 to 3 terapascal (1 TPa = 10^{12} Pa = 10 Mbar) into oxide phases but such pressures remain outside of the realm of high pressure experiments. In this work, we focus on the archetypal perovskite structure $CaTiO_3$, and investigate its phase diagram using the laser-heated diamond anvil cell technique coupled with *in situ* x-ray diffraction. At pressures above 60 GPa and temperatures up to 4500 K, we show evidence of the dissociation of $CaTiO_3$ into CaO and $CaTi_2O_5$ instead of a transformation into a denser post-perovskite phase. Similar decomposition schemes have been proposed for $MgSiO_3$ at ultra-high pressures in super-Earth's interiors; the decomposition reaction discovered here in $CaTiO_3$ could allow to better understand their consequences by providing a model amenable to experiments under accessible pressures.

1 Introduction

Bridgmanite, the orthorhombic (*Pbnm* space group) perovskite-structured compound with $(Mg,Fe)SiO_3$ composition is considered to be the most abundant mineral in the Earth's rocky mantle. This mineral undergoes a well-documented transition to a *Cmcm* $CaIrO_3$-type post-perovskite phase at approximately 120 GPa (Murakami et al. 2004; Oganov & Ono, 2004). For super-Earth modelling, it is important to investigate $MgSiO_3$ behaviour at much higher pressures and temperatures. Atomistic calculations have predicted that $MgSiO_3$

dissociates between 1 to 3 TPa into simple oxides MgO and SiO_2 or more complex assembly of denser silicates and oxides (Mg_2SiO_4, $MgSi_2O_5$) (Umemoto et al., 2011, 2017, 2019 and references therein; Wu et al. 2014; Niu et al. 2015). However, such pressures remain outside of the realm of static high-pressure experiments and difficult to achieve together with relevant temperatures in dynamic compression experiments. Therefore, to experimentally acquire better knowledge about these important mechanisms and transitions, another approach is to study analogue compounds. An analogue material usually mimics the crystallographic structure of the material while having a different composition. Several compounds such as $CaRhO_3$, $MgGeO_3$, $NaMgF_3$, $GdFeO_3$ and much more have been identified as model structures to explore high-density high-pressure evolution of ABX_3 compounds (Xu et al., 2015 and references herein). In this work, we focus on the mineral called perovskite (and archetypal perovskite structure) $CaTiO_3$, which can be interesting to compare with the perovskite-structured materials of rocky planets such as $MgSiO_3$ and $CaSiO_3$ perovskite. Since $CaTiO_3$ has the *Pbnm* orthorhombic perovskite structure at ambient conditions, it is expected to undergo structural transitions at more moderate pressures than bridgmanite or $CaSiO_3$. It has been also predicted that $CaTiO_3$ may undergo a series of transition perovskite (Pv) – post-perovskite (pPv) – post-post perovskite (ppPv) (Xu et al. 2015) that makes of this compound a very interesting case to study.

Perovskite and post-perovskite structures have been extensively studied during these past few years both by *ab initio* calculations and experiments (e.g. Murakami et al., 2004; Hirose et al., 2017 and references therein; Dutta et al., 2019; Umemoto et al., 2011, 2017, 2019; Xu et al., 2015; Tsuchiya et al., 2004). For $CaTiO_3$, first-principles calculations by Xu and al. (2015) propose that the *Pbnm* perovskite structure transforms to a post-perovskite *Cmcm* $CaIrO_3$ phase at 32.7 GPa, followed by another transition to a post-post-perovskite structure at 71.7 GPa. Using diamond anvil cells at room-temperature, it has been demonstrated by Guennou et al. (2010) that $CaTiO_3$ remains under the *Pnma* (or equivalent *Pbnm*) orthorhombic perovskite structure up to 60 GPa. With $CaTiO_3$, we focus on a class of materials in which the structural distortion is dominated by tilts of BO_6 octahedra (Zhao et al. 2011). It is interesting to identify the point where this structure destabilizes, for instance when the tilt angle ceases to evolve and bond compression becomes the main structural modification. The absence of heating in Guennou et al. (2010) may have, possibly, retained a metastable structure at the highest pressures. A dynamic compression study (Trunin et al.

1971) suggested a phase change in $CaTiO_3$ at 60 GPa without giving any structural information for the new state.

In the present study, we investigate the phase diagram of calcium titanate $CaTiO_3$ perovskite using the laser-heated diamond anvil cell technique coupled with *in situ* x-ray diffraction. We report the results of experiments conducted up to 170 GPa and temperatures up to 4500 K. We measure the thermal equation of state of the *Pbnm* orthorhombic perovskite phase. We also observe a gradual dissociation of $CaTiO_3$ into oxides instead of transformations into post-perovskite or post-post-perovskite phases.

2 Methods

2.1 X-ray diffraction experiment

The *in-situ* experiments were carried out at the ID27 beamline at the European Synchrotron Radiation Facility (ESRF) using laser-heated diamond anvil cell (LH-DAC) methods. We characterised the samples using powder x-ray diffraction in angle-dispersive mode using an MCCD detector (Mezouar et al. 2005; Mezouar et al, 2017). In this setup, the laser heating system is composed of two high-power diode-pumped Nd-YAG infrared lasers entering the DAC from both sides with an angle of 20°. Temperatures were measured by multi-wavelength spectral radiometry methods (Schultz et al. 2005). The working wavelength was 0.3738 Å (i.e., 33 keV) and remained the same during the whole experiment. We conducted eight runs in total (Table 1) with two types of starting materials. The first three runs were done using commercial synthetic $CaTiO_3$ (purchased from Kurt J. Lesker Company with a purity of 99.9%), grinded and loaded without any pressure transmitting medium but with platinum black powder that served as IR laser heating absorber as well as pressure calibrant (series #1, #2 and #3). The following four runs were carried out with a natural $CaTiO_3$ sample (Collection of Minerals, Sorbonne University, courtesy from J.C. Boulliard) compressed between KCl disks acting as thermal insulating pressure medium and pressure calibrant (series #4, #5, #6 and #7). X-ray diffraction patterns collected at ambient conditions confirmed the orthorhombic structure and the purity of the $CaTiO_3$ sample, with an excellent match with reference diffraction patterns obtained on a single crystal by Guennou et al. (2010). In the natural $CaTiO_3$ samples, trace elements in the crystal structure enabled significant YAG laser (1.064 µm) absorption and heating. The last experimental run was conducted with a natural $CaTiO_3$ sample loaded with neon as a pressure medium and a small piece of gold was added for pressure measurements (series #8).

X-ray diffraction images were collected on a MAR165 2D-CCD detector with exposure time of the order of 30 seconds at ambient temperature conditions, and up to 90 seconds at the most extreme conditions. Each CCD image was then processed with the DIOPTAS software (Prescher & Prakapenka, 2015) to obtain intensity versus 2-theta angle integrated patterns. These patterns were subsequently treated using the FullProf Suite software (Rodriguez-Carvajal, 2001) with a Le Bail refinement. Pressures corresponding to each diffractogram were calculated using different equations of state of platinum (Matsui et al. 2009), gold (Takemura & Dewaele, 2008) and KCl (Dewaele et al. 2012), as described in supplementary materials. The EoSFit program (Angel et al., 2014; Gonzales-Plata et al., 2016) was used to fit the thermal equation of state parameters of $CaTiO_3$ with the perovskite *Pbnm* structure.

2.2 Melting experiment

To provide additional information on the high-pressure behaviour of $CaTiO_3$, we performed *in situ* laser-heated diamond anvil cell experiments to determine the melting curve of $CaTiO_3$ up to 60 GPa. These experiments were carried out at IMPMC laboratory, Sorbonne University. Single pieces of synthetic $CaTiO_3$ (same sample as in the run #1-3 Table 1) were loaded in DACs equipped with anvils of 200 and 300 µm culet sizes to reach pressures ranging between 16 and 55 GPa. The sample chamber drilled in the pre-indented Re-gasket of the DAC assembly was loaded with sample pieces of about 10-20 µm thicknesses which were sandwiched between the pressure medium discs of KCl of 10-20 µm thickness. KCl acted as pressure transmitting medium, but also as a thermal insulator and chemical barrier between the sample and the diamond anvils. A ruby sphere was placed at the edge of the sample chamber to measure pressure with ruby fluorescence. Pressures were measured before and after each heating run. Our experimental setup is equipped with one-sided CO_2 laser heating system which is built with a Synrad Evolution 125 CO_2 laser delivering a gaussian beam (wavelength 10.6 µm, $M^2 < 1.2$) focused by a ZnSe lens on the sample through the diamond in an axial geometry (focal length 25 mm). The use of a CO_2 laser permits to heat non-metallic samples (*i.e.*, wide bandgap insulating materials) such as $CaTiO_3$ without any additional laser absorber such as Pt black. Heating is also effective across the entire thickness of the sample, with lesser axial temperature gradient (Smith et al., 2018). Temperature measurements were performed by spectro-radiometry, *i.e.* the analysis of thermal emission of the sample in the visible region (from 500 to 800 nm). The imaging and pyrometry system was made of a two-mirrors Schwarzschild reflective objective lens (focal 850 mm) used to

make an image of the hot spot on the entrance slit of the spectrometer (Acton 500i) equipped with an Andor-CDD camera. Optical pyrometry in the 500-800 nm range typically yields Planck's law fits within 10 K (uncertainty of the fit), which corresponds to an actual temperature uncertainty of about 130 K when emissivity changes and temperature variation are taken into account. Melting was detected by observation of a discontinuity in the curve of temperature vs laser power. This discontinuity in the absorption of the laser radiation, appears as a sudden increase of temperature at a given laser power, temperature which reaches then a so called 'plateau' attributed to melting. In few cases the laser power was slowly increased until the temperature reached a stable value ("plateau") due to melting at a given pressure (*e.g.* Boehler, 2000; Pradhan et al., 2015; Geballe & Jeanloz, 2012). We managed to fit the melting points using both the Kraut-Kennedy equation (Kraut & Kennedy, 1966) and the Simon equation (Simon, 1937). The formulation of the Kraut-Kennedy equation is:

(1)

$$T_m = T_m^0 \left(1 + C\frac{\Delta V}{V_0}\right)$$

with T_m the melting temperature at a given pressure and T_m^0 is the melting temperature at 1 atm. C is a constant depending on the material. The isothermal dilatation $\Delta V/V_0$ is defined as:

(2)

$$\frac{\Delta V}{V_0} = \frac{V_0 - V}{V}$$

where V_0 is the volume at ambient pressure and temperature.

The Simon equation is formulated as:

(3)

$$P_m = A\left[\left(\frac{T_m}{T_m^0}\right)^B - 1\right]$$

with T_m the melting temperature at a given pressure and T_m^0 is the melting temperature at 1 atm. A and B are constants that depend on the material.

3 Results and discussion

3.1 $CaTiO_3$ thermal equation of state

To establish the thermal equation of state of $CaTiO_3$ perovskite, we used different data sets. Guennou et al. (2010) provide a reliable equation of state at ambient temperature up to 60 GPa obtained by single crystal x-ray diffraction using fluorescence of ruby as pressure gauge and helium as pressure-transmitting medium. However, above 40 GPa, they noticed a broadening of the peaks in the diffraction pattern attributed to a non-hydrostatic compression of the single crystal sample. Accordingly, we only included their data from 0 to 40 GPa in the refinement. In this work, we present a room-temperature dataset that can be compared to Guennou et al. (2010) in the same pressure range. The two datasets agree up to 47 GPa and we discuss below the evolution at higher pressures.

We coupled the Guennou et al. (2010) results with our data obtained up to temperatures in excess of 3000 K at 60 GPa. Most of the dataset comes from the series with platinum (see "Data EoS" in repository 10.17632/nmkzfcdh/5.3). In the refinement process, we avoided to include data that showed signs of structural transition to other phases (typically above 60 GPa). We also used the most recent data from Yashima et al. (2009) in the refinement. This work established the high-temperature thermal expansion of $CaTiO_3$ perovskite and temperature-induced transition processes at ambient pressure up to 1720 K by neutron diffraction and Rietveld analysis refinement.

The refinement at T_0 = 300 K was achieved with the software EoSFit (Angel et al., 2014) using a third order Birch-Murnaghan equation of state:

(4)

$$P(V,T_0) = \frac{3}{2}K_0\left[\left(\frac{V}{V_0}\right)^{-\frac{7}{3}} - \left(\frac{V}{V_0}\right)^{-\frac{5}{3}}\right]\left[1 + \frac{3}{4}(K_0' - 4)\left[\left(\frac{V}{V_0}\right)^{-\frac{2}{3}} - 1\right]\right]$$

V_0 is the lattice volume at 300 K, V is the volume at a pressure point, K_0 is the bulk modulus and K'_0 is the first pressure derivative of the bulk modulus ($\partial K/\partial P$).

In order to determine the pressure considering the temperature we introduced a thermal pressure term, according to:

(5)

$$P^{tot}(V,T) = P(V,T_0) + P^{th}(V,T)$$

To determine the thermal pressure, we used a Berman model:

(6)

$$\alpha \approx \alpha_0 + \alpha_1(T - T_0)$$

α is the thermal expansion. Once the thermal expansion is calculated, we have to consider a temperature dependent bulk modulus written as:

(7)

$$K_T = K_0 + \frac{\partial K}{\partial T}(T - T_0)$$

Then, the thermal pressure can be expressed as:

(8)

$$P^{th}(V,T) = \int_{T_0}^{T} \alpha K_T dT$$

The results are presented in Table 2 and Figure 1a. Our preferred model is V_0 = 33.62 cm^3/mol/f.u., K_0 = 180.6 GPa, K'_0 = 4, α_0 = 3.245*10^{-5} K^{-1}, α_1 = 1.254*10^{-8} K^{-2} and $\partial K/\partial T$ = -0.022 GPa.K^{-1}. All parameters were refined simultaneously except V_0 which was fixed to the value reported by Guennou et al. (2010) which was obtained with high precision measurement on a single crystal. The refined K'_0 was found very close to 4 (4.06). We decided to fix it to 4 in the final refinement process.

We also calculated the relative error between the volume measured during the experiments and obtained by refining the diffraction patterns and the volume calculated with the obtained equation of state. The minimum and maximum error we obtained were 0.7% and -1.2%, respectively, which corresponds to a volume difference of approximately 0.199 and -0.334 cm^3/mol/f.u. (Figure 1b). The median error of our data is -0.07%. Thus, we can consider that the parameters of the thermal equation of state of $CaTiO_3$ are well defined with a χ^2 of 1.03.

By comparing our P-V-T data to other thermal equation of states, we extend the $CaTiO_3$ dataset to higher pressure and temperature and find a good agreement with other perovskite structures (Table 3). Our results on the thermal equation of state are comparable to thermoelastic parameters from other $CaTiO_3$ perovskite studies (Guennou et al. 2010, Webb et al. 1999, Kung & Rigden 1997, Fischer et al. 1993) done with different techniques (i.e.

ultrasonic interferometer, single crystal XRD in LH-DAC and powder XRD in LH-DAC) and extend the studied pressure range. The bulk modulus obtained in the present study is slightly higher but in good agreement with other studies (Webb et al. 1999). They found the same dK/dT as in the present study; however, they refined their thermal equation of state with constant thermal expansion (α_0) at ambient pressure whereas we include a temperature dependence term (α_0 and α_1) for a better fit. When refined with a constant thermal expansivity at 1 bar for comparison, we obtain a value of the same order (α=3.80 10^{-5} K^{-1}) as in Webb et al. (1999). Compared to other titanate perovskites (such as $SrTiO_3$ or $BaTiO_3$) (Guennou et al. 2010, Pruzan et al. 2002, Webb et al. 1999, Fischer et al. 1993), $CaTiO_3$ is less compressible than $SrTiO_3$ and $BaTiO_3$, which can be at first order a consequence of the cation size.

Importantly, when compared to other perovskite structures present in the Earth mantle (*i.e.*, $MgSiO_3$, $CaSiO_3$) (Tange et al. 2012, Ricolleau et al. 2009, Fiquet et al. 2000, Shim et al. 2000), $CaTiO_3$ is more compressible but its compressibility diminishes less than $MgSiO_3$ and $CaSiO_3$ as temperature increases.

These data have implications for planetary science. They confirm that perovskite-structured titanates are less incompressible than perovskite-structured silicates (table 2) opening an interesting crystal-chemical perspective to better understand the effect of substitutions of silicon in the perovskite octahedral site. Moreover, such measurements open the way to a future thermodynamic modeling of $CaTiO_3$ perovskite at high pressure and temperature which might have some relevance to better understand the behaviour of titanium at lower mantle conditions.

3.2 Orthorhombic and cubic perovskite structures of $CaTiO_3$

At ambient pressure and high temperature, the orthorhombic *Pbnm* phase of $CaTiO_3$ is stable up to 1500K (± 30K) (Naylor & Cook, 1946; Guyot et al., 1993; Redfern, 1996; Yashima & Ali, 2009) and further transforms into a cubic phase (space group *Pm-3m*) at higher temperature. At ambient temperature and high-pressure, Guennou et al. (2010) observed that the *Pbnm* structure was stable at least up to 60 GPa, a pressure range that we have extended up to 110 GPa in the present study (Figure 2a). However, we observe a discontinuity of the c axis in the compression behaviour of the orthorhombic perovskite *Pbnm* structure at 60 GPa with a change in slope of the evolution of the unit cell parameter as a function of pressure (Figure 2b). Each cell parameter was obtained from a LeBail fit to our diffractograms using the FullProf software. In figure 2b, cell parameters are presented in a

pseudo-cubic lattice geometry for easier comparison. This discontinuity in compression cannot be ascribed to non-hydrostaticity in the Ne pressure medium which has no reported rheological nor phase change in this pressure range, but rather reveals a change in compression mechanism, possibly associated to a thermodynamic path that progressively drives the perovskite structure outside its stability field. At room-temperature though, it is likely that energetic barriers cannot be easily overcome to reach a new thermodynamic stable state. Up to 60 GPa in Figure 2b, $CaTiO_3$ is still stable. Above 90 GPa, a axis becomes almost incompressible. Also, b axis remains constant on nearly the whole compression up to 100 GPa. However, it is clear that c axis experiences a change in compression above 60 GPa. It is striking to note that these changes in the compression slopes correspond to pressures at which a major transition is observed in $CaTiO_3$ at high pressure and temperature (see below). Such behaviour has been described in other systems: a strongly distorted metastable phase is described for instance in cold compressed forsterite (Finkelstein et al., 2014).

The structure of the orthorhombic *Pbnm* perovskite is made of tilted TiO_6 octahedra and of strongly distorted CaO_{12} dodecahedral sites. It is known from many studies (Glazer, 1972; Andrault & Poirier, 1991; Angel et al., 2005) that tilt and distortions change as a function of pressure and temperature and that the orthorhombic structure tends to transform to a cubic structure with increasing temperature. At pressure below 60 GPa, as temperature increases, we indeed observe a transformation of the *Pbnm* orthorhombic $CaTiO_3$ perovskite into a more symmetric cubic structure (Figure 3). However, in most diffraction patterns, we still detect relics of the orthorhombic structure mixed with the cubic phase. These relics are seen in the form of a doubling of the peaks corresponding to the cubic phase with no appearance of the orthorhombic peaks between 2.5 Å (10°2θ) and 1.9 Å (11.5°2θ) and can be attributed to a gradient of temperature during the experiment. A tetragonal phase (*I4/mcm*) has been reported in literature (e.g., Guyot et al., 1993; Redfern, 1996; Yashima & Ali, 2009) at intermediate temperatures between orthorhombic and cubic phases. Its restricted temperature stability range may however explain why it was not observed in the present study. According to Redfern (1996) or Yashima & Ali (2009), the existence of a tetragonal phase (*I4/mcm*) between the perovskite and the cubic domain is shown in the diffractograms by the disappearance of the *Pbnm* reflections 120, 210, 121 and 103 in the d-spacing range between 2.37 and 2.10 Å, which only leaves the 211 reflection. It is clear from our diffractograms that the 211 reflection was never observed, so we conclude that either the tetragonal phase only exists in a narrow range of temperature that we missed here, or alternatively that the

tetragonal domain no longer exists at high pressure. A similar transition detailed by Komabayashi et al. (2007) is observed in $CaSiO_3$ perovskite which transforms to a $Pm\bar{3}m$ cubic phase, from a *I4/mcm* tetragonal phase, with a slightly positive dT/dP slope (1.1 K/GPa) and at relatively low temperature (≈ 500 K) compared to $CaTiO_3$ in the same range of pressure. The study also shows that the incorporation of aluminium stabilizes the tetragonal phase to higher temperature (Kurashina et al. 2004). Thomson et al. (2019) found the same stabilization process with the incorporation of titanium in $CaSiO_3$ which brings an interesting analogy between $CaTiO_3$ and $CaSiO_3$.

By comparing the measured unit cell parameters of the cubic perovskite phase of $CaTiO_3$ and those calculated using the thermal equation of state of the orthorhombic perovskite, we found that the cubic phase is slightly smaller than the *Pbnm* phase extrapolated at these temperatures (≈ 3500K). Indeed, the difference between the calculated and measured volume of the cubic phase, using the perovskite thermal equation of state in the same condition, is around -8% in volume (Table S1).

3.3 Melting of $CaTiO_3$ perovskite

Several studies have attempted to determine the melting temperature of $CaTiO_3$ at ambient pressure providing estimates ranging between 2188 K and 2262 K (Coughanour et al., 1954; DeVries et al., 1954; R. S. Roth, 1958, Jongejean & Wilkins, 1970; V. Daněk & I. Nerád, 2002). To anchor the melting curve at 1 bar, we have retained the value provided by Coughanour et al., i.e. 2188 K which was also selected by Robie et al. 1978.
In Figure 4, we present the fitted solid-liquid line using two models for comparison, one from Kraut & Kennedy, 1966 and one from Simon, 1937.

(9)

$$T_m = 2188 * \left[1 + 4.23 * \left(\frac{\Delta V}{V_0}\right)\right] \quad (Kraut - Kennedy)$$

(10)

$$Pm = 65.66 * \left[\left(\frac{T_m}{T_0}\right)^{1.05} - 1\right] \quad (Simon)$$

Residuals of the two fits are given in Table S2.

Those melting results are compared with published experimental or calculated melting curves of $MgSiO_3$ (Zerr & Boehler, 1993; DiPaola & Brodholt, 2016) and $CaSiO_3$ (Zerr et al., 1997; Braithwaite & Stixrude, 2019) silicate perovskites. As shown in Figure 4, in the pressure range between 20 and 60 GPa, the melting curve of bridgmanite determined using a liquid-solid interface atomistic simulations (DiPaola & Brodholt, 2016) is indeed very close to the experimental melting curve of $CaTiO_3$. However, the experimental data from Zerr & Boehler (1993) suggest a different behaviour of $MgSiO_3$ with a steeper slope and higher melting temperatures. $CaSiO_3$ perovskite has a higher melting temperature than other perovskites and it has been determined both experimentally using CO_2 LH-DAC (Zerr et al., 1997) and using DFT calculations (Braithwaite & Stixrude, 2019). Experimental slopes of melting curves of $MgSiO_3$ and $CaSiO_3$ appear steeper than in $CaTiO_3$. Unfortunately, to our best knowledge, no other melting studies on titanates (i.e. $BaTiO_3$, $SrTiO_3$ $MnTiO_3$) at high pressure and temperature have been conducted. Therefore, the present work provides the first insights on the melting of titanate perovskites at high pressures.

It is interesting to note that our results on melting of $CaTiO_3$ perovskite under pressure suggest that titanate and silicate perovskites have melting temperatures of the same order of magnitude which could imply relatively weak dependencies of the melting temperature of mantle perovskites upon substitution of silicon in the octahedral sites. But these speculations remain to be confirmed experimentally and by ab initio simulations.

3.4 Dissociation of $CaTiO_3$ into CaO and $CaTi_2O_5$.

At pressures exceeding 50-60 GPa, x-ray diffraction patterns of $CaTiO_3$ perovskite drastically change upon heating (Figure 5), which suggests a transition to another phase or an assemblage of new phases. We first analysed the high pressure diffractograms ranging from 90 to 170 GPa which showed no traces left of the former *Pbnm* orthorhombic initial perovskite structure. We used the tool DICVOL (Louër & Boultif, 2004) in the FullProf Suite to test several possible structures (space groups *Pmmm*, *Pnma*, $P2_1/m$, $P2_1/c$, *Pcca*, etc). We also tried to index those diffractograms with a post-perovskite $CaIrO_3$-type *Cmcm* phase, as observed for instance in $MgSiO_3$, but we could not find any satisfactory match with the data. We also extended our research by testing other structures found in high-pressure ABX_3 systems before or after dissociation (cotunnite, brookite, baddeleyite, pseudobrookite, stibnite, $CaSi_2O_5$, Ca_2SiO_4, $SrSi_2O_5$, Fe_2P, etc) but again, without any satisfying results. The best fit was obtained using a *P2/m* space group for all diffractograms over the whole pressure range

including high temperature and quenched to ambient temperature data. This lattice volume is of around 300 $Å^3$. This volume is much larger than any unit cell volumes of $CaTiO_3$ extrapolated to those conditions (≈ 170 $Å^3$), thus indicating that the stoichiometry is different from $CaTiO_3$. Along these lines, this volume of 300 $Å^3$ would perfectly match a stoichiometric volume of CaO + $CaTi_2O_5$ in those conditions.

In all high-temperature diffractograms at pressures above 90 GPa, two reflections are also consistent with a CaO-*B2* phase, according to the equation of state for *B2*-phase of CaO (Yamanaka et al., 2002) corrected for temperatures. One example of the refinement is given in Figure 6, where the two co-existing phases can be identified in that pressure domain.

Interestingly enough, CaO transforms from NaCl-*B1* to CsCl-*B2* structures at around 60 GPa at 300 K (Richet et al. 1988, Yamanaka et al. 2002), which corresponds to the pressure under which $CaTiO_3$ starts to transform into the *P2/m* phase. Accordingly, we think the dissociation is likely driven by the change in structure of CaO.

Following these observations reinforced by an analogy with Wu et al. (2009) who have suggested dissociation of a $FeTiO_3$ perovskite into $(Fe_{1-\delta},Ti_\delta)O$ and $Fe_{1+\delta}Ti_{2-\delta}O_5$, we propose that above 60 GPa and at high temperature, $CaTiO_3$ indeed breaks down into CaO (*B2*) and $CaTi_2O_5$ instead of going through a pPv phase, following the dissociation reaction:

(11)

$$CaTiO_3 \rightarrow ½\ CaO + ½\ CaTi_2O_5$$

To validate this hypothesis, we notice that in addition to those of the *P2/m* phase and of *B2* - CaO, we cannot observe any diffraction line of TiO_2. The summary of the $CaTiO_3$ phases observed at different pressures and temperatures are all represented in a data-plot diagram in Figure 7a and a tentative phase diagram Figure 7b.

This dissociation of the perovskite $CaTiO_3$ without going through a post-perovskite phase is an important experimental demonstration of the importance of simple oxides for the thermodynamic evolution of ABX_3 systems. Tsuchiya et al. (2015) predicted a new Fe_2P-type phase for cotunnite-SiO_2 around 0.9 TPa which could impact ABX_3 structures by favoring their dissociations in the silicate mantles ($MgSiO_3$, $CaSiO_3$) of super-Earths. Also, there is still no evidence of a $CaIrO_3$-type post-perovskite phase in $CaSiO_3$ up to 149 GPa (Fujino et al. 2009). Though, the appearance of such a complex oxide as $CaTi_2O_5$ is a transformation

that has similarities with the prediction made for $MgSiO_3$ and the stabilization of $MgSi_2O_5$ at extreme conditions, according to Umemoto et al. (2011, 2017).

In every high-pressure transition from a perovskite to a post-perovskite phase or to an assemblage containing oxides, a negative volume variation of around 1-2% has been observed (e.g., Hirose et al., 2005 and references therein). Considering the stoichiometry of equation (11), the volume of $CaTiO_3$, extrapolated to high-pressure and high-temperature (≈164Å), is slightly higher than that of ½ CaO + ½ $CaTi_2O_5$ (≈156Å) in the same conditions. Using our high-pressure high-temperature equation of state of $CaTiO_3$ and that of CaO as B2 (Yamanaka et al., 2002), we infer that the volume variation of reaction (11) is between -1% and -5% depending on the temperature. Although a high-pressure polymorph of $CaTiO_3$ with $CaIrO_3$ structure was predicted by first-principles calculations (Xu et al., 2015), the results of the present experimental study suggest that breakdown according to reaction (8) bypasses the expected post-perovskite phase and that dissociation to two other phases is favoured.

Between 60 and 90 GPa, the $CaTiO_3$ perovskite structure can still be recognized in our patterns in coexistence with an assemblage of CaO-*B2* and $CaTi_2O_5$-*P2/m*. The $CaTiO_3$ reflections weaken while the reflections attributed to $CaTi_2O_5$ grow with increasing pressure. In this transition pressure range, however, few peaks remain unidentified. They could be due to yet unidentified defect structures derived from $CaTiO_3$ perovskite, in a manner possibly similar to those reported in $MgSiO_3$ by Tschauner et al. (2008). Another important aspect of this transition mechanism is the effect of temperature on the dissociation process given in equation (11). At ambient temperature, the cold compression of $CaTiO_3$ is unable to overcome energy barriers needed to drive the transition into CaO and $CaTi_2O_5$. We observe instead a change in the compression regime of the lattice parameters. As temperature is increased, the main peaks of the *P2/m* phase start to appear but this new phase still coexists with $CaTiO_3$ perovskite for kinetic reasons over a 30 GPa pressure range. It is important to note that the complex mixed phase regime appearing in Figure 7 is prohibited according to thermodynamics and thus, draws its origin in kinetic effects.

Other authors have also addressed the complexity of different transition processes in ABO_3 compounds. Wu et al. (2009) have shown that ilmenite $FeTiO_3$ goes through a perovskite phase but then dissociates into a wüstite-type $(Fe_{1-\delta},Ti_\delta)O$ and a monoclinic *C2/c* $Fe_{1+\delta}Ti_{2-\delta}O_5$ structure, thus omitting the post-perovskite phase. More recently, Akaogi et al. (2016) proposed a dissociation of $FeTiO_3$ into Fe_2TiO_4 + TiO_2 or Fe_2TiO_4 + $FeTi_2O_5$

depending on the temperature. They also highlighted the dissociation process of $ZnTiO_3$ (Akaogi et al. 2015) where the ilmenite structure transforms into a perovskite and then dissociates directly into its simpler oxides with a rocksalt-type ZnO and a baddeleyite-type TiO_2. Kojitani et al. (2005) studied the dissociation of $SrSiO_3$ into Sr_2SiO_4 and $SrSi_2O_5$ at 16 GPa and proceeded with a Rietveld analysis of the obtained species. In 2010, Okada et al. (2010) found in $MnTiO_3$ the same process of decomposition as shown in the present study for $CaTiO_3$ but with an orthorhombic $MnTi_2O_5$ structure with lattice parameters indeed close to those of $FeTi_2O_5$ from Akaogi et al. (2016). In addition, Kondo et al. (2000) described a high-pressure phase transition in MnO from *B1* to a distorted *B1* at 30 GPa, which echoes with the dissociation of $MnTiO_3$ into MnO and $MnTi_2O_5$.

These data show that titanates tend to dissociate more easily without going through a post-perovskite phase whereas germanates adopt more easily post perovskite phases. (Ito & Matsui, 1979). Tateno et al. (2006) describe a transition from perovskite to a $CaIrO_3$-type post-perovskite phase in $MnGeO_3$ at 60 GPa and 1800 K, exactly the same process as in $MgGeO_3$ at 63 GPa and 1800 K (Hirose et al., 2005). More recently, $ZnGeO_3$ also joined the Pv-pPv transition group with a similar process as $MgSiO_3$ as it transforms around 114 GPa (Yusa et al., 2014). In 2017, However, Dutta et al. triggered the dissociation of $FeGeO_3$ into FeO and GeO_2 at high temperature without adopting a pPv structure, following the same transition path as in $FeSiO_3$ (Dutta et al., 2017).

Based on those literature observations and on the experimental data of the present study, we thus confirm that when chemical bonding characteristics are met as it is the case in titanates, ABO_3 systems often break down into different oxides compounds. As the dissociation of $CaTiO_3$ (Pv) without transition to a post-perovskite phase is a phenomenon that has already been seen in other ABO_3 systems, it further brings us to the conclusion that this type of transition is common, especially in $ATiO_3$ systems (table 4). Moreover, according to Akaogi et al. (2016) (and references therein), it seems that the titanate perovskites do not transform into post-perovskite but instead dissociate into oxides, a behaviour seemingly related to a small degree of covalency of Ti-O bonds.

4 Implications for planetary interiors

It is interesting to compare our observation of the dissociation of $CaTiO_3$ with the prediction by Umemoto et al. (2011) using atomistic calculations of a dissociation of $MgSiO_3$ into MgO and $MgSi_2O_5$ phase with a $P2_1/c$-type structure at pressures of the order of 900

GPa. Moreover, Tsuchiya & Tsuchiya (2015) predicted the dissociation of $CaSiO_3$ and $MgSiO_3$ into their corresponding oxides, with the change in structure of SiO_2 as a possible cause, which echoes with the dissociation of $CaTiO_3$ likely favored by the CaO *B1-B2* transformation.

To summarize, the decomposition of several perovskites (titanates, germanates and silicates) under pressure is often observed into a combination of their simplest constitutive oxides (AO and BO_2). However, a thorough examination of the literature reveals more complex stoichiometries of these breakdowns. With $CaTiO_3$, these transformations and dissociations can be observed in a pressure range accessible to accurate experimental studies which could usefully shed light on certain aspects of the evolution of $MgSiO_3$ or $CaSiO_3$ compounds at ultra-high pressures in exoplanets. Moreover, further detailed study of the $CaTi_2O_5$ phase could usefully shed light on some properties of ASi_2O_5 compounds in super-Earth mantles

5 Conclusion

In conclusion, we explored the high-pressure high temperature transformations of $CaTiO_3$ perovskite up to 170 GPa and 4500 K. We measured the thermal equation of state in the stability domain of $CaTiO_3$ perovskite. We also measured the melting curve of this perovskite up to 55 GPa. At higher pressures and temperatures, at odds with what had been predicted by theoretical calculations, we show that $CaTiO_3$ does not transform into a post-perovskite $CaIrO_3$ *Cmcm* structure but instead dissociates into *B2*-CaO and monoclinic $CaTi_2O_5$. The transition process starts at 60 GPa and is spread, for kinetic reasons, over a large range of pressure. The transition toward *B2*-CaO and $CaTi_2O_5$ is complete at pressures around 100 GPa.

Strengthening knowledge of the evolution of ABX_3 structures at high pressures is of first importance to infer the mineralogical state of exoplanetary mantles. We propose that future studies of the $CaTi_2O_5$ phase discovered in this work in a pressure range amenable to precise experimental studies will provide insights into exoplanetary ultra-high pressure phenomena that are still beyond reach of experimental mineral physics studies.

Acknowledgments

We would like to thank Lucas Maurice for a first report of the experimental dataset and raw diffraction pattern, Benoit Baptiste for his help and advice about X-ray pattern

refinements and structural identification. B. Truffet, G. Fiquet, G. Morard, M.A. Baron, F. Miozzi and M. Harmand have received funding from the European Research Council (ERC) under the European Union's Horizon 2020 research and innovation program (grant agreement 670787). The datasets are available in the following repository in Mendeley Data: http://dx.doi.org/10.17632/nmkzfcdh75.3

References

Akaogi, M., Abe, K., Yusa, H., Ishii, T., Tajima, T., Kojitani, H., … Inaguma, Y. (2016). High-pressure high-temperature phase relations in $FeTiO_3$ up to 35 GPa and 1600 °C. *Physics and Chemistry of Minerals*, ***44***(1), 63–73. doi:10.1007/s00269-016-0836-3

Akaogi, M., Abe, K., Yusa, H., Kojitani, H., Mori, D., & Inaguma, Y. (2015). High-pressure phase behaviors of $ZnTiO_3$: ilmenite–perovskite transition, decomposition of perovskite into constituent oxides, and perovskite–lithium niobate transition. *Physics and Chemistry of Minerals*, ***42***(6), 421–429. doi:10.1007/s00269-015-0733-1

Andrault, D., & Poirier, J. (1991). Evolution of the distortion of perovskites under pressure: An EXAFS study of $BaZrO_3$, $SrZrO_3$ and $CaGeO_3$. *Physics and Chemistry of Minerals*, ***18***(2), 91–105. doi:10.1007/bf00216602

Angel, R. J., Alvaro, M., & Gonzalez-Platas, J. (2014). EosFit7c and a Fortran module (library) for equation of state calculations. *Zeitschrift für Kristallographie - Crystalline Materials*, ***229***(5). doi:10.1515/zkri-2013-1711

Angel, R. J., Zhao, J., & Ross, N. L. (2005). General Rules for Predicting Phase Transitions in Perovskites due to Octahedral Tilting. *Physical Review Letters*, ***95***(2). doi:10.1103/physrevlett.95.025503

Basmajian, J. A., & Devries, R. C. (1957). Phase Equilibria in the System $BaTiO_3$-$SrTiO_3$. *Journal of the American Ceramic Society*, ***40***(11), 373–376. doi:10.1111/j.1151-2916.1957.tb12556.x

Boehler, R. (2000). Laser heating in the diamond cell: Techniques and applications. *Hyperfine Interactions*, ***128***(1-3), 307–321. doi:10.1023/A:1012648019016

Braithwaite, J., & Stixrude, L. (2019). Melting of $CaSiO_3$ perovskite at high pressure. *Geophysical Research Letters*, *46*(4), 2037–2044. https://doi.org/10.1029/2018gl081805

Coughanour, L., Roth, R., & Deprosse, V. (1954). Phase equilibrium relations in the systems Lime-Titania and Zirconia-Titania. *Journal of Research of the National Bureau of Standards*, ***52***(1), 37. doi:10.6028/jres.052.007

Daněk, V. & Nerád, I. (2002) Phase Diagram and Structure of Melts of the System CaO-TiO_2-SiO_2. *Chemical Paper* **56**(4)**,** 241–246.

Devries, R. C., Roy, R., & Osborn, E. F. (1954). Phase Equilibria in the System CaO-TiO_2-SiO_2. *The Journal of Physical Chemistry*, ***58***(12), 1069–1073. doi:10.1021/j150522a005

Dutta, R., Greenberg, E., Prakapenka, V. B., & Duffy, T. S. (2019). Phase transitions beyond post-perovskite in $NaMgF_3$ to 160 GPa. *Proceedings of the National Academy of Sciences*, ***116***(39), 19324–19329. doi:10.1073/pnas.1909446116

Dutta, R., Tracy, S. J., Stan, C. V., Prakapenka, V. B., Cava, R. J., & Duffy, T. S. (2017). Phase stability of iron germanate, FeGeO3, to 127 GPa. *Physics and Chemistry of Minerals*, ***45***(4), 367–379. https://doi.org/10.1007/s00269-017-0927-9

Fei, Y., Ricolleau, A., Frank, M., Mibe, K., Shen, G., & Prakapenka, V. (2007). Toward an internally consistent pressure scale. *Proceedings of the National Academy of Sciences*, ***104***(22), 9182–9186. doi:10.1073/pnas.0609013104

Finkelstein, G. J., Dera, P. K., Jahn, S., Oganov, A. R., Hall, C. M., Meng, Y., & Duffy, T. S. (2014). *Phase transitions and equation of state of forsterite to 90 GPa from single-crystal X-ray diffraction and molecular modeling*, ***99***(1), 35–43. doi:10.2138/am.2014.4526

Fischer, G., Wang, Z., & Karato, S.-I. (1993). Elasticity of $CaTiO_3$, $SrTiO_3$ and $BaTiO_3$ perovskites up to 3.0 Gpa: the effect of crystallographic structure. *Physics and Chemistry of Minerals*, ***20***(2), 97–103. doi:10.1007/bf00207202

Fujino, K., Nishio-Hamane, D., Suzuki, K., Izumi, H., Seto, Y., & Nagai, T. (2009). Stability of the perovskite structure and possibility of the transition to the Post-perovskite structure in $CaSiO_3$, $FeSiO_3$, $MnSiO_3$ and $CoSiO_3$. *Physics of the Earth and Planetary Interiors*, ***177***(3-4), 147–151. https://doi.org/10.1016/j.pepi.2009.08.009

Geballe, Z. M., & Jeanloz, R. (2012). Origin of temperature plateaus in laser-heated diamond anvil cell experiments. *Journal of Applied Physics*, ***111***(12), 123518. doi:10.1063/1.4729905

Glazer, A. M. (1972). The classification of tilted octahedra in perovskites. *Acta Crystallographica Section B Structural Crystallography and Crystal Chemistry*, ***28***(11), 3384-3392. doi:10.1107/s0567740872007976

Gonzalez-Platas, J., Alvaro, M., Nestola, F., & Angel, R. (2016). EosFit7-GUI: A new graphical user interface for equation of state calculations, analyses and teaching. *Journal of Applied Crystallography*, ***49***(4), 1377-1382. doi:10.1107/s1600576716008050

Guennou, M., Bouvier, P., Kreisel, J., & Machon, D. (2010). Pressure-temperature phase diagram of $SrTiO_3$ up to 53 GPa. *Physical Review B,* ***81***(5). doi:10.1103/physrevb.81.054115

Guennou, M., Bouvier, P., Krikler, B., Kreisel, J., Haumont, R., & Garbarino, G. (2010). High-pressure investigation of $CaTiO_3$ up to 60 GPa using x-ray diffraction and Raman spectroscopy. *Physical Review B,* ***82***(13). doi:10.1103/physrevb.82.134101

Guyot, F., Richet, P., Courtial, P., & Gillet, P. (1993). High-temperature heat capacity and phase transitions of $CaTiO_3$ perovskite. *Physics and Chemistry of Minerals,* ***20***(3), 141-146. doi:10.1007/bf00200116

Hirose, K. (2005). Clapeyron slope of the post-perovskite phase transition in $CaIrO_3$. *Geophysical Research Letters,* ***32***(13). doi:10.1029/2005gl023219

Hirose, K., Kawamura, K., Ohishi, Y., Tateno, S., & Sata, N. (2005). Stability and equation of state of $MgGeO_3$ post-perovskite phase. *American Mineralogist*, ***90***(1), 262–265. https://doi.org/10.2138/am.2005.1702

Hirose, K., Sinmyo, R., & Hernlund, J. (2017). Perovskite in Earth's deep interior. *Science,* ***358***(6364), 734-738. doi:10.1126/science.aam8561

Ito, E., & Matsui, Y. (1979). High-pressure transformations in silicates, germanates, and titanates with ABO3 stoichiometry. *Physics and Chemistry of Minerals*, ***4***(3), 265–273. https://doi.org/10.1007/bf00307950

Jongejan, A., & Wilkins, A. (1970). A re-examination of the system CaO-TiO_2 at liquidus temperatures. *Journal of the Less Common Metals*, ***20***(4), 273-279. doi:10.1016/0022-5088(70)90001-9

Kojitani, H., Kido, M., & Akaogi, M. (2005). Rietveld analysis of a new high-pressure strontium silicate $SrSi_2O_5$. *Physics and Chemistry of Minerals,* ***32***(4), 290-294. doi:10.1007/s00269-005-0467-6

Komabayashi, T., Hirose, K., Sata, N., Ohishi, Y., & Dubrovinsky, L. S. (2007). Phase transition in casio3 perovskite. *Earth and Planetary Science Letters*, ***260***(3-4), 564–569. https://doi.org/10.1016/j.epsl.2007.06.015

Kondo, T., Yagi, T., Syono, Y., Noguchi, Y., Atou, T., Kikegawa, T., & Shimomura, O. (2000). Phase transitions of MnO to 137 GPa. *Journal of Applied Physics*, ***87***(9), 4153-4159. doi:10.1063/1.373045

Kraut, E. A., & Kennedy, G. C. (1966). New Melting Law at High Pressures. *Physical Review Letters*, ***16***(14), 608-609. doi:10.1103/physrevlett.16.608

Kung, J., & Rigden, S. (1999). Oxide perovskites: Pressure derivatives of the bulk and shear moduli. *Physics and Chemistry of Minerals*, ***26***(3), 234-241. doi:10.1007/s002690050182

Kurashina, T., Hirose, K., Ono, S., Sata, N., & Ohishi, Y. (2004). Phase transition in Al-bearing CASIO3 perovskite: Implications for Seismic discontinuities in the lower mantle. *Physics of the Earth and Planetary Interiors*, *145*(1-4), 67–74. https://doi.org/10.1016/j.pepi.2004.02.005

Liu, Z., Yan, J., Duan, S., Sun, X., Zhang, C., & Guo, Y. (2010). The melting curve of perovskite under lower mantle pressures. *Solid State Communications*, ***150***(13-14), 590-593. doi:10.1016/j.ssc.2009.12.038

Louër, D., & Boultif, A. (2006). Indexing with the successive dichotomy method, DICVOL04. *Ninth European Powder Diffraction Conference*, ***23***, 225-230. doi:10.1524/9783486992526-039

Mezouar, M., Crichton, W. A., Bauchau, S., Thurel, F., Witsch, H., Torrecillas, F., . . . Borel, C. (2005). Development of a new state-of-the-art beamline optimized for monochromatic single-crystal and powder X-ray diffraction under extreme conditions at the ESRF. *Journal of Synchrotron Radiation*, ***12***(5), 659-664. doi:10.1107/s0909049505023216

Mezouar, M., Giampaoli, R., Garbarino, G., Kantor, I., Dewaele, A., Weck, G., . . . Bauchau, S. (2017). Methodology for in situ synchrotron X-ray studies in the laser-heated diamond anvil cell. *High Pressure Research*, ***37***(2), 170-180. doi:10.1080/08957959.2017.1306626

Murakami, M., Hirose, K., Kawamura, K., Sata, N., & Ohishi, Y. (2004). Post-Perovskite Phase Transition in $MgSiO_3$. *Science*, ***304(***5672), 855-858. doi:10.1126/science.1095932

Naylor, B. F., & Cook, O. A. (1946). High-Temperature Heat Contents of the Metatitanates of Calcium, Iron and Magnesium. *Journal of the American Chemical Society*, ***68***(6), 1003-1005. doi:10.1021/ja01210a030

Niu, H., Oganov, A. R., Chen, X., & Li, D. (2015). Prediction of novel stable compounds in the Mg-Si-O system under exoplanet pressures. *Scientific Reports*, ***5***(1). doi:10.1038/srep18347

Oganov, A. R., & Ono, S. (2004). Theoretical and experimental evidence for a post-perovskite phase of $MgSiO_3$ in Earth's D″ layer. *Nature, **430***(6998), 445-448. doi:10.1038/nature02701

Okada, T., Yagi, T., & Nishio-Hamane, D. (2010). High-pressure phase behavior of $MnTiO_3$: Decomposition of perovskite into MnO and $MnTi_2O_5$. *Physics and Chemistry of Minerals, **38(***4), 251-258. doi:10.1007/s00269-010-0400-5

Ono, S., Brodholt, J. P., & Price, G. D. (2011). Elastic, thermal and structural properties of platinum. *Journal of Physics and Chemistry of Solids, **72***(3), 169-175. doi:10.1016/j.jpcs.2010.12.004

Paola, C. D., & Brodholt, J. P. (2016). Modeling the melting of multicomponent systems: the case of $MgSiO_3$ perovskite under lower mantle conditions. *Scientific Reports*, ***6***(1). doi:10.1038/srep29830

Pradhan, G. K., Fiquet, G., Siebert, J., Auzende, A., Morard, G., Antonangeli, D., & Garbarino, G. (2015). Melting of MORB at core–mantle boundary. *Earth and Planetary Science Letters, **431***, 247-255. doi:10.1016/j.epsl.2015.09.034

Prescher, C., & Prakapenka, V. B. (2015). DIOPTAS: A program for reduction of two-dimensional X-ray diffraction data and data exploration. *High Pressure Research, **35***(3), 223-230. doi:10.1080/08957959.2015.1059835

Pruzan, P., Gourdain, D., Chervin, J., Canny, B., Couzinet, B., & Hanfland, M. (2002). Equation of state of $BaTiO_3$ and $KNbO_3$ at room temperature up to 30GPa. *Solid State Communications, **123***(1-2), 21-26. doi:10.1016/s0038-1098(02)00201-6

Redfern, S. A. (1996). High-temperature structural phase transitions in perovskite. *Journal of Physics: Condensed Matter, **8***(43), 8267-8275. doi:10.1088/0953-8984/8/43/019

Richet, P., Mao, H., & Bell, P. M. (1988). Static compression and equation of state of CaO to 1.35 Mbar. *Journal of Geophysical Research: Solid Earth, **93***(B12), 15279-15288. doi:10.1029/jb093ib12p15279

Robie, R. A., Hemigway, B. S. & Fisher, J. R. (1979). Thermodynamic properties of minerals and related substances at 298.15 K and 1 bar (10^5 Pascals) pressure and at higher temperatures. *U.S. Geological Survey*, 253–254. doi:10.3133/b2131

Rodríguez-Carvajal, J. (2001). Recent Developments of the Program FULLPROF, in Commission on Powder Diffraction (IUCr). *Newsletter* **26**, 12-19 (2001).

Roth, R. (1958). Revision of the phase equilibrium diagram of the binary system calcia-titania, showing the compound $Ca_4Ti_3O_{10}$. *Journal of Research of the National Bureau of Standards,* ***61***(5), 437-440. doi:10.6028/jres.061.037

Schultz, E., Mezouar, M., Crichton, W., Bauchau, S., Blattmann, G., Andrault, D., . . . Loubeyre, P. (2005). Double-sided laser heating system forin situhigh pressure–high temperature monochromatic x-ray diffraction at the esrf. *High Pressure Research,* ***25***(1), 71-83. doi:10.1080/08957950500076031

Smith, D., Smith, J. S., Childs, C., Rod, E., Hrubiak, R., Shen, G., & Salamat, A. (2018). A CO2 laser heating system for in situ high pressure-temperature experiments at HPCAT. *Review of Scientific Instruments*, ***89***(8), 083901. https://doi.org/10.1063/1.5040508

Simon, F. (1937). On the range of stability of the fluid state. *Transactions of the Faraday Society,* ***33***, 65-73. doi:10.1039/tf9373300065

Sun, T., Umemoto, K., Wu, Z., Zheng, J., & Wentzcovitch, R. M. (2008). Lattice dynamics and thermal equation of state of platinum. *Physical Review B,* ***78***(2), 024304. doi:10.1103/physrevb.78.024304

Takemura, K., & Dewaele, A. (2008). Isothermal equation of state for gold with a He-pressure medium. *Physical Review B,* ***78***(10), 104119. doi:10.1103/physrevb.78.104119

Tateno, S., Hirose, K., Sata, N. & Ohishi, Y. (2005). High-pressure behavior of MnGeO3 and CdGeO3 perovskites and the post-perovskite phase transition. *Physics and Chemistry of Minerals*, ***32***(10), 721–725. https://doi.org/10.1007/s00269-005-0049-7

Thomson, A. R., Crichton, W. A., Brodholt, J. P., Wood, I. G., Siersch, N. C., Muir, J. M., Dobson, D. P., & Hunt, S. A. (2019). Seismic velocities of casio3 perovskite can explain LLSVPs In Earth's lower mantle. *Nature*, ***572***(7771), 643–647. https://doi.org/10.1038/s41586-019-1483-x

Tschauner, O., Kiefer, B., Liu, H., Sinogeikin, S., Somayazulu, M., & Luo, S. (2008). Possible structural polymorphism in Al-bearing magnesiumsilicate post-perovskite. *American Mineralogist*, ***93***(4), 533-539. doi:10.2138/am.2008.2372

Tsuchiya, T., & Tsuchiya, J. (2011). Prediction of a hexagonal SiO_2 phase affecting stabilities of $MgSiO_3$ and $CaSiO_3$ at multimegabar pressures. *Proceedings of the National Academy of Sciences*, ***108***(4), 1252–1255. https://doi.org/10.1073/pnas.1013594108

Tsuchiya, T., Tsuchiya, J., Umemoto, K., & Wentzcovitch, R. M. (2004). Phase transition in MgSiO3 perovskite in the earth's lower mantle. *Earth and Planetary Science Letters, **224***(3-4), 241-248. doi:10.1016/j.epsl.2004.05.017

Umemoto, K., & Wentzcovitch, R. M. (2019). Ab initio exploration of post-pPv transitions in low-pressure analogs of $MgSiO_3$. *Physical Review Materials, **3***(12), 123601. doi:10.1103/physrevmaterials.3.123601

Umemoto, K., & Wentzcovitch, R. M. (2011). Two-stage dissociation in $MgSiO_3$ post-perovskite. *Earth and Planetary Science Letters, **311***(3-4), 225-229. doi:10.1016/j.epsl.2011.09.032

Umemoto, K., Wentzcovitch, R. M., Wu, S., Ji, M., Wang, C., & Ho, K. (2017). Phase transitions in MgSiO3 post-perovskite in super-Earth mantles. *Earth and Planetary Science Letters, **478***, 40-45. doi:10.1016/j.epsl.2017.08.032

Webb, S., Jackson, I., & Gerald, J. F. (1999). Viscoelasticity of the titanate perovskites $CaTiO_3$ and $SrTiO_3$ at high temperature. *Physics of the Earth and Planetary Interiors, **115***(3-4), 259-291. doi:10.1016/s0031-9201(99)00081-3

Wu, S. Q., Ji, M., Wang, C. Z., Nguyen, M. C., Zhao, X., Umemoto, K., . . . Ho, K. M. (2013). An adaptive genetic algorithm for crystal structure prediction. *Journal of Physics: Condensed Matter, **26***(3), 035402. doi:10.1088/0953-8984/26/3/035402

Wu, X., Steinle-Neumann, G., Narygina, O., Kantor, I., Mccammon, C., Prakapenka, V., . . . Dubrovinsky, L. (2009). High-Pressure Behavior of Perovskite: $FeTiO_3$ Dissociation into $(Fe_{1-\delta},Ti_{\delta})O$ and $Fe_{1+\delta}Ti_{2-\delta}O_5$. *Physical Review Letters, **103***(6), 065503. doi:10.1103/physrevlett.103.065503

Xu, C., Xu, B., Yang, Y., Dong, H., Oganov, A. R., Wang, S., . . . Bellaiche, L. (2015). Prediction of a stable post-post-perovskite structure from first principles. *Physical Review B, **91***(2), 020101. doi:10.1103/physrevb.91.020101

Yamanaka, T., Kittaka, K., & Nagai, T. (2002). B1-B2 transition in CaO and possibility of $CaSiO_3$-perovskite decomposition under high pressure. *Journal of Mineralogical and Petrological Sciences, **97***(4), 144-152. doi:10.2465/jmps.97.144

Yashima, M., & Ali, R. (2009). Structural phase transition and octahedral tilting in the calcium titanate perovskite CaTiO3. *Solid State Ionics, **180***(2-3), 120-126. doi:10.1016/j.ssi.2008.11.019

Yusa, H., Tsuchiya, T., Akaogi, M., Kojitani, H., Yamazaki, D., Hirao, N., … Kikegawa, T. (2014). Postperovskite Phase Transition of ZnGeO3: Comparative Crystal Chemistry of Postperovskite Phase Transition from Germanate Perovskites. *Inorganic Chemistry*, ***53***(21), 11732–11739. https://doi.org/10.1021/ic501958y

Zerr, A., & Boehier, R. (1993). Melting of (Mg, Fe)SiO_3-Perovskite to 625 Kilobars: Indication of a High Melting Temperature in the Lower Mantle. *Science*, ***262***(5133), 553-555. doi:10.1126/science.262.5133.553

Zerr, A., Serghiou, G., & Boehler, R. (1997). Melting of $CaSiO_3$ perovskite to 430 kbar and first in-situ measurements of lower mantle eutectic temperatures. *Geophysical Research Letters*, ***24***(8), 909-912. doi:10.1029/97gl00829

Zhao, J., Ross, N. L., Wang, D., & Angel, R. J. (2011). High-pressure crystal structure of elastically isotropic CaTiO3 perovskite under hydrostatic and non-hydrostatic conditions. *Journal of Physics: Condensed Matter*, ***23***(45), 455401. https://doi.org/10.1088/0953-8984/23/45/455401

Supplementary References

Campbell, A. J., Danielson, L., Righter, K., Seagle, C. T., Wang, Y., & Prakapenka, V. B. (2009). High pressure effects on the iron–iron oxide and nickel–nickel oxide oxygen fugacity buffers. *Earth and Planetary Science Letters*, ***286***(3-4), 556–564. doi:10.1016/j.epsl.2009.07.022

Dewaele, A., Belonoshko, A. B., Garbarino, G., Occelli, F., Bouvier, P., Hanfland, M., & Mezouar, M. (2012). High-pressure–high-temperature equation of state of KCl and KBr. *Physical Review B*, ***85***(21). doi:10.1103/physrevb.85.214105

Dorogokupets, P. I., & Oganov, A. R. (2007). Ruby, metals, and MgO as alternative pressure scales: A semi empirical description of shock-wave, ultrasonic, x-ray, and thermochemical data at high temperatures and pressures. *Physical Review B*, ***75***(2). doi:10.1103/physrevb.75.024115

Matsui, M., Ito, E., Katsura, T., Yamazaki, D., Yoshino, T., Yokoyama, A., & Funakoshi, K. (2009). The temperature-pressure-volume equation of state of platinum. *Journal of Applied Physics*, ***105***(1), 013505. doi:10.1063/1.3054331

Takemura, K., & Dewaele, A. (2008). Isothermal equation of state for gold with a He-pressure medium. *Physical Review B*, ***78***(10), 104119. doi:10.1103/physrevb.78.104119

Tsuchiya, T., & Kawamura, K. (2002). First-principles electronic thermal pressure of metal Au and Pt. *Physical Review B*, ***66***(9), 094115. doi:10.1103/physrevb.66.094115

Zha, C., Mao, H., & Hemley, R. J. (2000). Elasticity of MgO and a primary pressure scale to 55 GPa. *Proceedings of the National Academy of Sciences*, ***97***(25), 13494-13499. doi:10.1073/pnas.240466697

Data references

Guennou, M., Bouvier, P., Krikler, B., Kreisel, J., Haumont, R., & Garbarino, G. (2010). High-pressure investigation of $CaTiO_3$ up to 60 GPa using x-ray diffraction and Raman spectroscopy. *Physical Review B,* ***82***(13). doi:10.1103/physrevb.82.134101

Truffet, B., Fiquet, G., Morard, G., Baron, A. M., Miozzi, F., Harmand, M., Ravasio, A., Mezouar, M., Guyot, F. (2021). Thermal equation of state and phase diagram of $CaTiO_3$ perovskite. *Mendeley Data*, V2, doi: 10.17632/nmkzfcdh75.3

Yashima, M., & Ali, R. (2009). Structural phase transition and octahedral tilting in the calcium titanate perovskite CaTiO3. *Solid State Ionics,* ***180***(2-3), 120-126. doi:10.1016/j.ssi.2008.11.019

Figures

a) b)

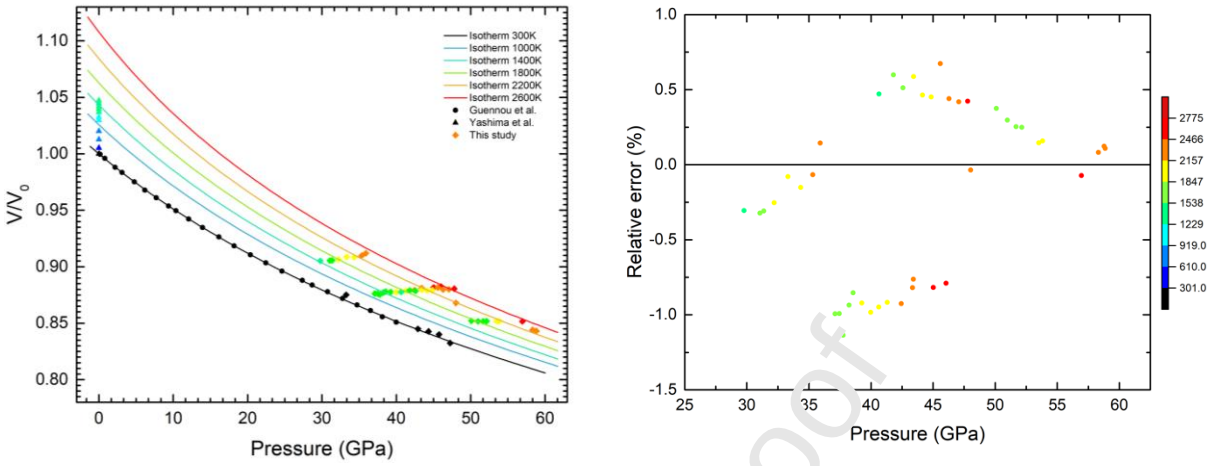

Figure 1: a) Thermal equation of state of $CaTiO_3$ perovskite with isotherms from 300 K to 2600 K, along with experimental data used in the refinement. This dataset includes: Guennou et al. (2010) data from 0 to 40 GPa (black dots), data from Yashima et al. (2008) at ambient pressure (represented by the coloured triangles), our own data collected at room-temperature from 40 to 47 GPa (black diamonds) and data collected at high-temperature from 30 to 60 GPa (coloured diamonds) b) Relative error between the volume calculated with the thermal EoS and the volume measured on each diffractograms. The colour scale corresponds to the measured temperatures in K.

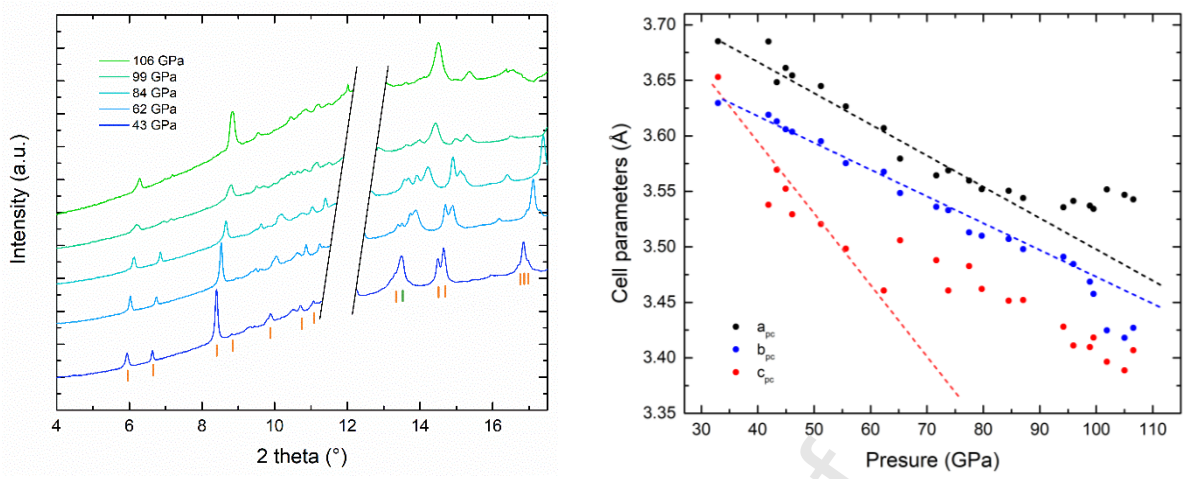

a) b)

Figure 2: a) Room temperature X-ray diffraction patterns of $CaTiO_3$ perovskite as a function of pressure with peak positions indicated in orange; the Ne pressure medium peak is marked in green and main peaks are masked so as to evidence details among lower intensity reflections; b) Room-temperature $CaTiO_3$ cell axis evolution as a function of pressure. Cell parameters are recalculated within a pseudo-cubic cell from the *Pbnm* structure where $a_{pc}=a_{pv}/\sqrt{2}$, $b_{pc}= b_{pv}/\sqrt{2}$, $c_{pc}=c_{pv}/2$ (pc: pseudo-cubic; pv: perovskite). The straight dotted lines are guide to the eye to evidence the change in the compression behavior. We observe a change in the slope at 90 GPa par axis a and b, and a change at 60 GPa for axis c.

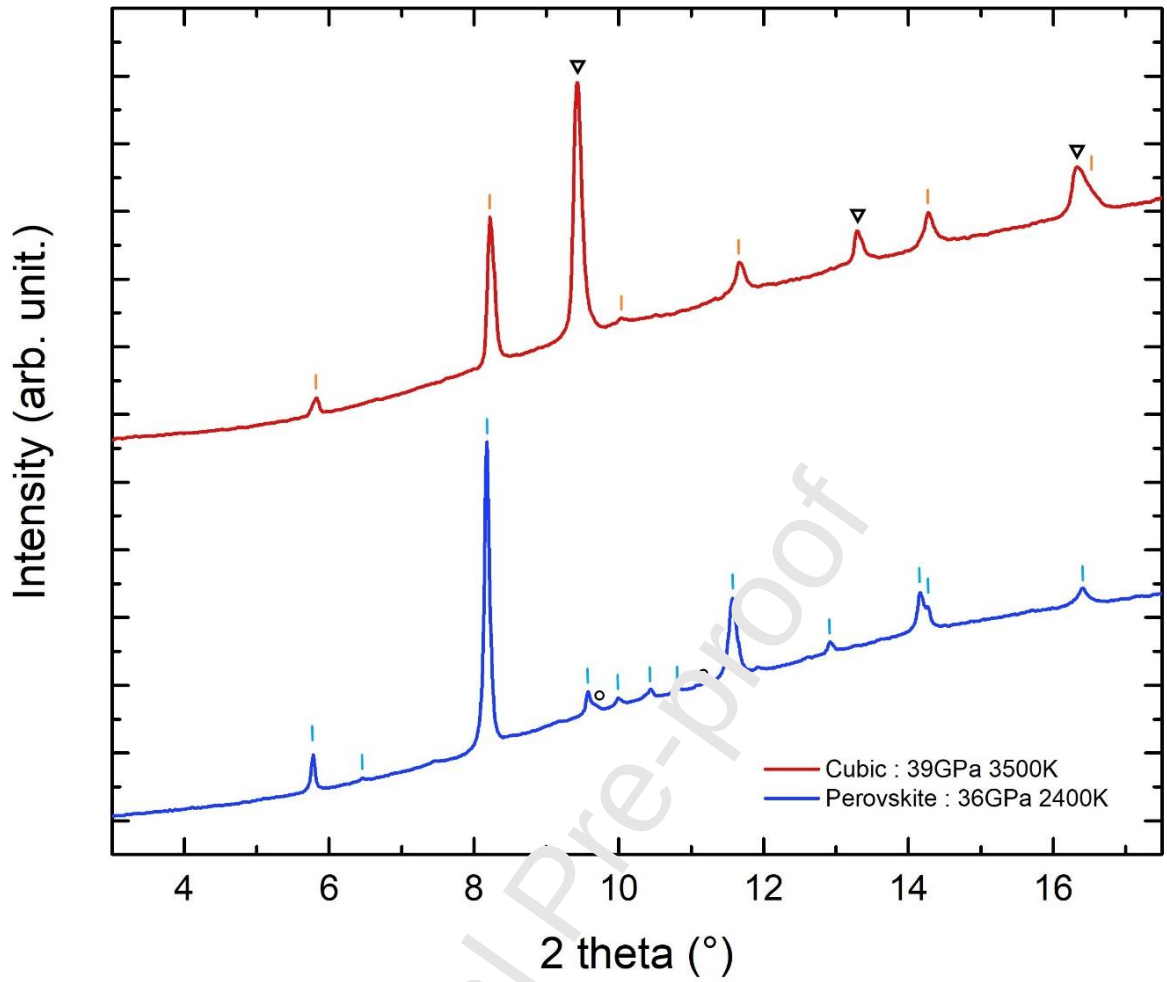

Figure 3: Orthorhombic perovskite to cubic structure transition. At the bottom, the perovskite (blue ticks) diffractogram with open circles corresponding to the platinum reflections. On top, the diffractogram of the cubic phase (orange ticks) with open triangles corresponding to the KCl reflections.

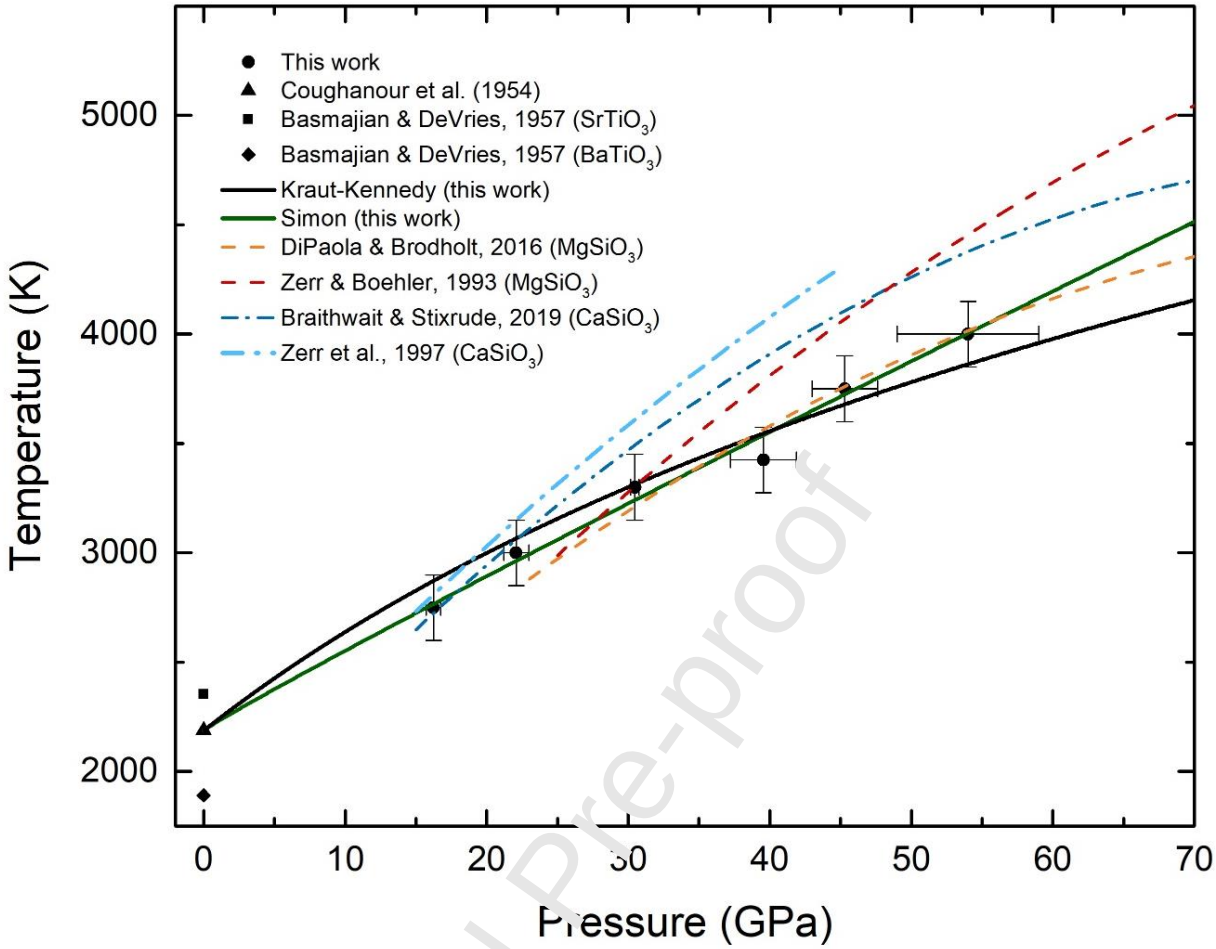

Figure 4: Our melting curve of $CaTiO_3$ plotted along with melting curves of $CaSiO_3$ and $MgSiO_3$ for comparison. The study from Zerr & Boehler (1993) and Zerr et al. (1997) have been also performed with DAC experiments, while the study from DiPaola & Brodholt (2016) and Braithwaite & Stixrude (2019) are from atomistic simulations. The black circular dots are our experimental data and the green and black lines are Simon's and Kraut-Kennedy's fits of our data points. The data at ambient pressure come from Coughanour et al. (1954) for $CaTiO_3$ and from Basmajian & DeVries (1957) for $SrTiO_3$ and $BaTiO_3$.

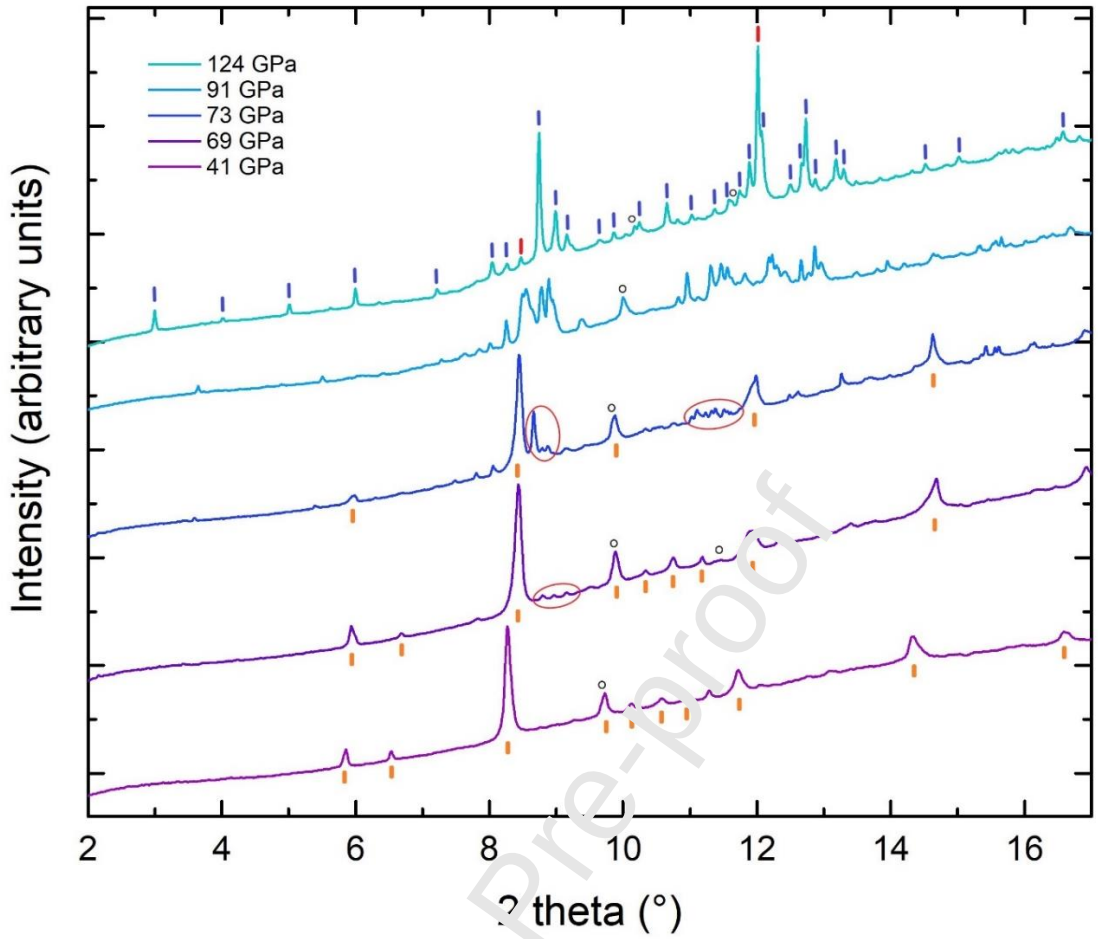

Figure 5: Examples of diffractograms at pressures from 41 to 124 GPa and temperature between 1500 K and 2500 K showing the evolution from pure $CaTiO_3$ at low pressures (orange ticks) to $CaTi_2O_5$ (blue ticks) + CaO (red ticks) mixture at the highest pressures. Open black circles represent the platinum. Open red circles show regions where new reflections are first observed, until we observe the full crystallisation of $CaTi_2O_5$ mixed with CaO at pressures above 100 GPa. The diffractogram at 76 GPa shows a coexistence between the $CaTiO_3$ perovskite phase and the appearance of what we assume are the reflections from the $CaTi_2O_5$ + CaO phase. The diffractogram at 91 GPa shows the reflections of the $CaTi_2O_5$ + CaO phase in formation but not fully formed due to kinetic reasons.

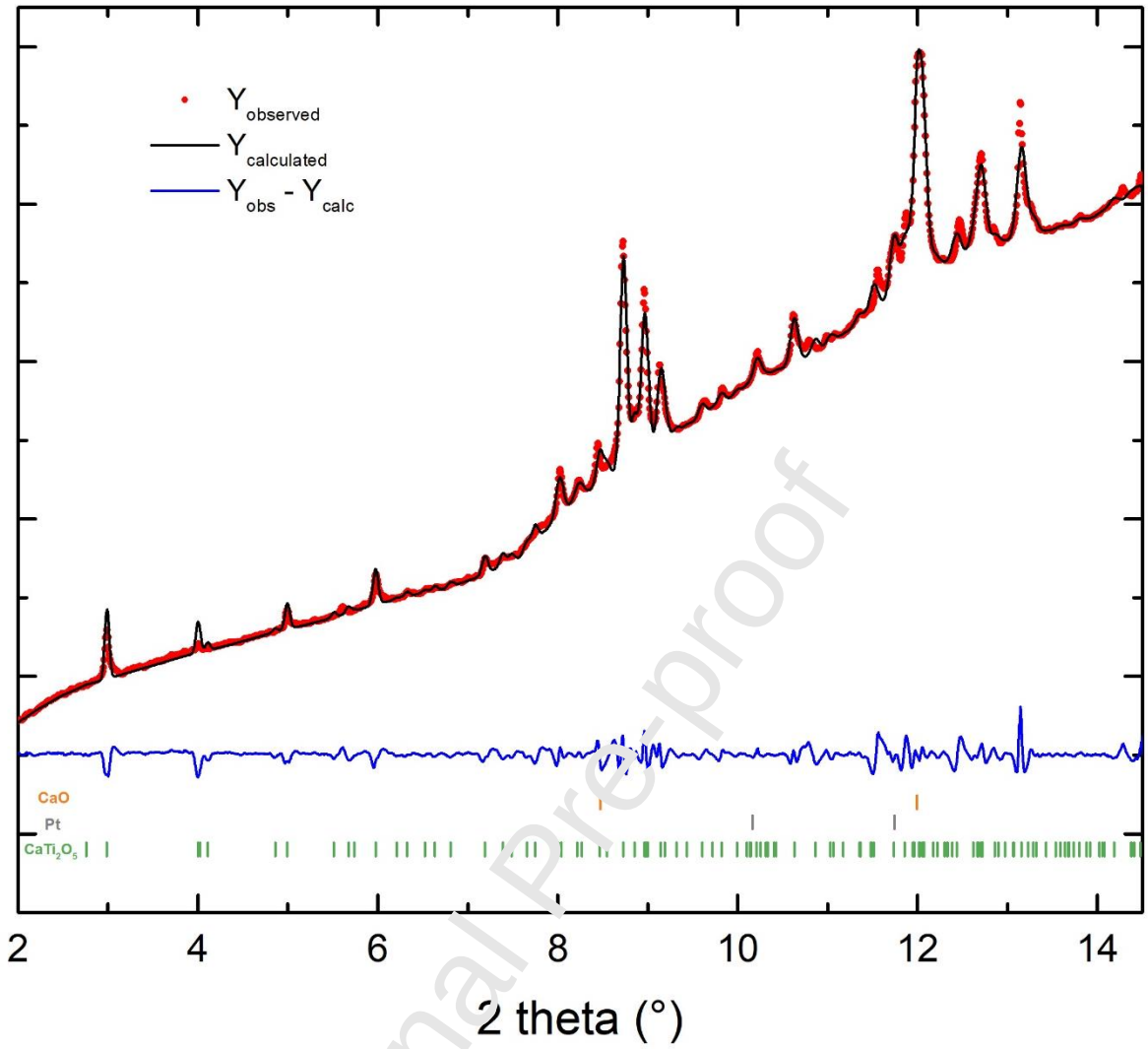

Figure 6: Full profile LeBail fit of a high-pressure diffraction pattern recorded at 122 GPa and 2900 K (series #2, Table 1). The green ticks correspond to *P2/m*-$CaTi_2O_5$ structure (a=7.78 Å, b=5.36 Å, c=7.18 Å and β=91.24°), the orange ticks to *B2*-CaO (a=2.53 Å) and the grey ticks correspond to the platinum (a=3.65 Å). χ^2 = 0.055. Formular unit Z=4. Data available here : 10.17632/rmkzfcdh75.3

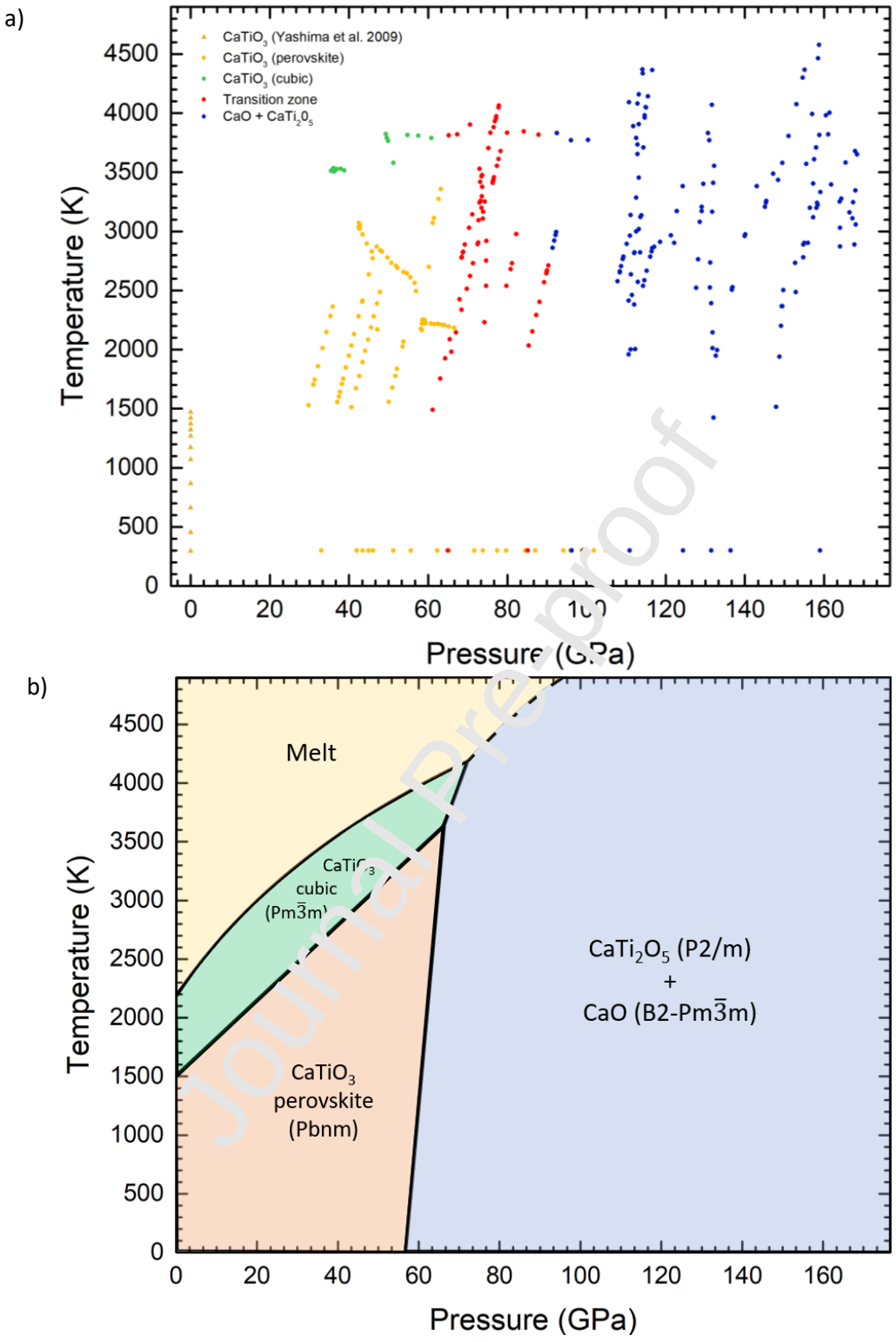

Figure 7: Summary of the $CaTiO_3$ phases observed at different pressures and temperatures.

a) Summary of XRD data collected at different pressures and temperatures. Yellow dots: $CaTiO_3$ orthorhombic (Pbnm) perovskite phase. Yellow triangles: neutron diffraction data from Yashima et al. (2009) at ambient pressure and up to 1500K. Green dots: $CaTiO_3$ cubic perovskite phase $Pm\bar{3}m$. Red symbols: mixed phase regime of kinetic

origin containing $CaTiO_3$ perovskite (Pbnm) together with a higher-pressure assemblage marked as blue dots when devoid of perovskite signal. This high-pressure assemblage consists of CaO (B2) and $CaTi_2O_5$ P2/m. Each pressure condition was measured either with KCl, platinum or gold pressure standards.

b) Tentative phase diagram of $CaTiO_3$, according to X-ray diffraction data collected in this study at different pressure-temperature and to previous literature data. The hypothetical phase boundaries have been drawn without fit, using data of figure 7a. The melting curve of $CaTiO_3$ perovskite was fitted with a Simon model. The tetragonal phase intermediate between orthorhombic and cubic perovskite structures was not represented.

Tables

Series #	$CaTiO_3$ type	Origin	Pressure transmitting medium	Pressure scale	Pressure domain (GPa)	Temperature domain (K)	Diamond culets
1	Powdered	Synthetic	$CaTiO_3$ + Pt	Pt	30 -78	1500 - 4000	150/300
2	Powdered	Synthetic	$CaTiO_3$ + Pt	Pt	83 - 120	2000 - 3000	100/300
3	Powdered	Synthetic	$CaTiO_3$ + Pt	Pt	121 - 155	2000 - 4400	250
4	Polycrystalline	Natural	KCl	KCl	35 – 75	2100 - 3500	200
5	Polycrystalline	Natural	KCl	KCl	47 – 115	2100 - 4400	100/300
6	Polycrystalline	Natural	KCl	KCl	127 - 161	1400 - 4000	100/300
7	Polycrystalline	Natural	KCl	KCl	154 - 168	2800 - 4500	150/300
8	Polycrystalline	Natural	Ne	Au	28 - 109	300	150/300

Table 1: Samples used for the different experimental runs.

V_0 (cm^3/mol/f.u.)	33.622 (fixed)
K_0 (GPa)	180.6 (4)
K'_0	4 (fixed)
dK/dT ($GPa.K^{-1}$)	-0.022 (1)
α_0 ($x10^{-5}$ K^{-1})	3.25 (5)
α_1 ($x10^{-8}$ K^{-2})	1.3 (1)

Table 2: Parameters of the thermal equation of state of $CaTiO_3$ (χ^2 = 1.03), with V_0 fixed and set to the value determined by Guennou et al. (2010) and K'_0 fixed to 4.

	V_0 (cm^3/mol/f.u.)	K_0 (Gpa)	K'_0	dK/dT (GPa K^{-1})	α_0 (10^{-5} K^{-1})	α_1 (10^{-8} K^{-2})
$CaTiO_3$						
This study	33.62 (7)[a]	180.6 (4)	4 (fixed)	-0.022 (1)	3.25 (5)	1.3 (1)
Guennou (2010)	33.62 (7)	181.0 (6)	4 (fixed)	-	-	-
Webb (1999)	33.82	172.1 (10)	6.09[b]	-0.0225 (7)	3.87	-
Kung (1997)	34.17 (2)	175	5.78	-	-	-
Fischer (1993)	33.87	177 (3)	5.1 (8)	-	-	-
$SrTiO_3$[*]						
Guennou (2010)	35.93 (1)	165 (3)	6.4 (8)	-	-	-
Webb (1999)	35.89	172.0 (1)	5.36[b]	-0.031 (1)	3.23 (2)[c]	-
Fischer (1993)	35.87	178.8 (46)	4.31 (1)	-	-	-
$BaTiO_3$[**]						
Pruzan (2002)	38.72	135	6.4	-	-	-
Fischer (1993)	38.74	139.2 (31)	9[d]	-	-	-
$MgSiO_3$						
Tange (2012)	24.45 (fixed)	256.7 (15)	4.09 (6)	-	-	-
Ricolleau (2009)	24.69 (fixed)	245 (1)	4 (fixed)	-0.036 (1)	3.19 (17)	0.88 (16)
Fiquet (2000)	24.43 (1)	259.5 (9)	3.69 (4)	-0.017 (2)	2.18 (12)	0.11 (8)
$CaSiO_3$						
Ricolleau (2009)	27.46 (fixed)	244 (1)	4 (fixed)	-0.035 (2)	3.06 (19)	0.87 (18)
Shim (2000)	27.45 (3)	236 (4)	3.9 (2)	-0.028 (11)	2.2 (3)	-

[a] From Guennou et al. (2010) – Room temperature DAC with x-ray diffraction.
[b] From Fischer et al. (1993) – Extrapolated from 500 MPa. Piston cylinder apparatus and ultrasonic interferometric technique.
[c] From de Ligny & Richet (1996) – Calorimetry and energy-dispersive x-ray diffraction.
[d] From Fischer & Polian (1987) – Brillouin scattering in DAC.
[*] Data for the cubic phase (0-10 GPa)
[**] Data for the tetragonal phase (0-2 GPa)

Table 3: Thermal equation-of-state parameters of different titanate, bridgmanite and calcium silicate perovskite.

Material	Pressure	geometry	a (Å)	b (Å)	c (Å)	β (°)	V (Å^3)
$CaTi_2O_5$	120 GPa	Monoclinic *P2/m*	7.776	5.362	7.167	91.29	298.75
	155 GPa	Monoclinic *P2/m*	7.662	5.268	7.049	91.422	284.43
$NaMg_2F_5$ (Dutta, 2019)	88 GPa	Monoclinic $P2_1/c$	5.618	4.977	7.729	89.23	197.08
	137 GPa	Monoclinic $P2_1/c$	5.423	4.732	7.312	89.2	187.62
$FeTi_2O_5$ (Akaogi, 2016)	31 GPa HT°	Orthorhombic	8.567	5.753	5.257	-	259.10
$MnTi_2O_5$ (Okada, 2010)	61 GPa HT°	Orthorhombic	8.263	5.743	5.179	-	245.77
$FeTi_2O_5$ (Wu, 2009)	40 GPa HT°	Monoclinic *C2/c*	10.135	4.305	10.023	141.48	272.37
$SrSi_2O_5$ (Kojitani, 2005)	16 GPa HT°	Orthorhombic *Cmca*	5.239	9.280	13.441	-	653.47

Table 4: Comparison of the AB_2X_5 structures and lattice parameters.

Author statement

Baptiste Truffet: Validation, Formal analysis, Investigation, Writing – Original Draft, Writing – Review & Editing, Visualization.

Guillaume Fiquet: Conceptualization, Methodology, Validation, Investigation, Writing – Original Draft, Supervision, Project administration, Funding acquisition.

Guillaume Morard: Validation, Investigation.

Marzena A. Baron: Validation, Investigation.

Francesca Miozzi: Validation, Investigation

Marion Harmand: Validation, Investigation.

Alessandra Ravasio: Validation, Investigation.

Mohamed Mezouar: Validation, Investigation, Resources.

François Guyot: Conceptualization, Methodology, Validation, Investigation, Writing – Original Draft, Writing – Review & Editing, Supervision, Project administration.

Declaration of interests

The authors declare that they have no known competing financial interests or personal relationships that could have appeared to influence the work reported in this paper.

Graphical abstract

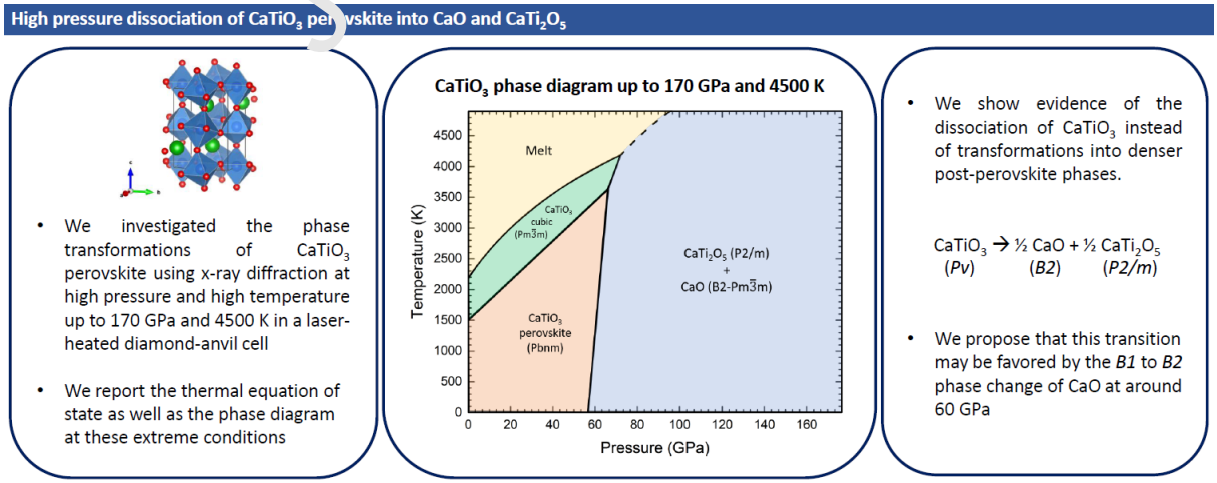

Highlights:

- Phase diagram of the calcium titanate perovskite $CaTiO_3$ up to 170 GPa and 4500 K.
- Thermal equation of state of the orthorhombic (*Pbnm*) perovskite $CaTiO_3$.
- Dissociation of the $CaTiO_3$ perovskite into CaO and $CaTi_2O_5$ without going through a post-perovskite phase.